J|A|C|S
ARTICLES
Published on Web 04/27/2007

Acetylcholinesterase: Mechanisms of Covalent Inhibition of Wild-Type and H447I Mutant Determined by Computational Analyses

Yuhui Cheng,*,† Xiaolin Cheng,† Zoran Radić,‡ and J. Andrew McCammon†,‡

Contribution from the Howard Hughes Medical Institute, Department of Chemistry and Biochemistry, and Department of Pharmacology, University of California at San Diego, La Jolla, California 92093-0365

Received January 26, 2007; E-mail: ycheng@mccammon.ucsd.edu

Abstract: The reaction mechanisms of two inhibitors *TFK*$^+$ and *TFK*^{0} binding to both the wild-type and H447I mutant mouse acetylcholinesterase (mAChE) have been investigated by using a combined *ab initio* quantum mechanical/molecular mechanical (QM/MM) approach and classical molecular dynamics (MD) simulations. In the wild-type mAChE, the binding reactions of *TFK*$^+$ and *TFK*^{0} are both spontaneous processes, which proceed through the nucleophilic addition of the Ser203-O_γ to the carbonyl-C of *TFK*$^+$ or *TFK*^{0}, accompanied with a simultaneous proton transfer from Ser203 to His447. No barrier is found along the reaction paths, consistent with the experimental reaction rates approaching the diffusion-controlled limit. By contrast, *TFK*$^+$ binding to the H447I mutant may proceed with a different reaction mechanism. A water molecule takes over the role of His447 and participates in the bond breaking and forming as a "charge relayer". Unlike in the wild-type mAChE case, Glu334, a conserved residue from the catalytic triad, acts as a catalytic base in the reaction. The calculated energy barrier for this reaction is about 8 kcal/mol. These predictions await experimental verification. In the case of the neutral ligand *TFK*^{0}, however, multiple MD simulations on the *TFK*^{0}/H447I complex reveal that none of the water molecules can be retained in the active site as a "catalytic" water. Furthermore, our alchemical free energy calculation also suggests that the binding of *TFK*^{0} to H447I is much weaker than that of *TFK*$^+$. Taken together, our computational studies confirm that *TFK*^{0} is almost inactive in the H447I mutant and also provide detailed mechanistic insights into the experimental observations.

1. Introduction

Acetylcholinesterase (AChE, EC 3.1.1.7) is a hydrolytic enzyme that belongs to the serine hydrolase family. It plays important roles during the course of signal transmission at cholinergic synapses. The principal biological role of acetylcholinesterase is the termination of impulse transmissions by rapidly hydrolyzing the neurotransmitter, acetylcholine (ACh).[1−3] Dysfunctions of AChE or other components of cholinergic synapses are involved in several human diseases, including myasthenia gravis, glaucoma, Alzheimer's, and Parkinson's diseases.[4−9] As a result, AChE has become an important target for rational drug design.

The crystal structure of AChE is characterized by a deep narrow gorge which penetrates halfway into the enzyme and contains the catalytic site located near the bottom, *ca.* 20 Å deep.[10] Kinetic studies have revealed that AChE possesses a remarkably high activity, with an ACh turnover rate of about 10^4 s^{-1} under physiological conditions, approaching the diffusion-controlled limit.[11−13]

Similar to many other proteases, the catalytic triad in AChE consisting of Ser203(200),[14] His447(440), and Glu334(327) is believed to be essential to hydrolysis. Each of these three residues has a specific role in generating the nucleophilic potential at the seryl O_γ. The replacement of any of them with Ala can cause at least 3300-fold of activity loss.[15] The detailed

† Howard Hughes Medical Institute, Department of Chemistry and Biochemistry.
‡ Department of Pharmacology.

(1) Rosenberry, T. L. *Adv. Enzymol. Relat. Areas Mol. Biol.* **1975**, *43*, 103−218.
(2) Schumacher, M.; Camp, S.; Maulet, Y.; Newton, M.; Macpheequigley, K.; Taylor, S. S.; Friedmann, T.; Taylor, P. *Fed. Proc.* **1986**, *45*, 2976−2981.
(3) Taylor, P. *The Pharmacological Basis of Therapeutics*; MacMillan: New York, 1985.
(4) Contestabile, A.; Fila, T.; Bartesaghi, R.; Contestabile, A.; Ciani, E. *J. Neurochem.* **2006**, *97*, 515−526.
(5) Piazzi, L.; Rampa, A.; Bisi, A.; Gobbi, S.; Belluti, F.; Cavalli, A.; Bartolini, M.; Andrisano, V.; Valenti, P.; Recanatini, M. *J. Med. Chem.* **2003**, *46*, 2279−2282.
(6) Bachurin, S. O. *Med. Res. Rev.* **2003**, *23*, 48−88.
(7) Sramek, J. J.; Zarotsky, V.; Cutler, N. R. *Drug Dev. Res.* **2002**, *56*, 347−353.
(8) Kryger, G.; Silman, I.; Sussman, J. L. *Struct. Fold. Des.* **1999**, *7*, 297−307.
(9) Egan, T. M.; North, R. A. *Nature* **1986**, *319*, 405−407.
(10) Sussman, J. L.; Harel, M.; Frolow, F.; Oefner, C.; Goldman, A.; Toker, L.; Silman, I. *Science* **1991**, *253*, 872−879.
(11) Bazelyansky, M.; Robey, E.; Kirsch, J. F. *Biochemistry* **1986**, *25*, 125−130.
(12) Hasinoff, B. B. *Biochim. Biophys. Acta* **1982**, *704*, 52−58.
(13) Nolte, H. J.; Rosenberry, T. L.; Neumann, E. *Biochemistry* **1980**, *19*, 3705−3711.
(14) Amino acids and numbers refer to mouse or human AChE, and the numbers in parentheses refer to the positions of analogous residues in TcAChE.
(15) Shafferman, A.; Kronman, C.; Flashner, Y.; Leitner, M.; Grosfeld, H.; Ordentlich, A.; Gozes, Y.; Cohen, S.; Ariel, N.; Barak, D.; Harel, M.; Silman, I.; Sussman, J. L.; Velan, B. *J. Biol. Chem.* **1992**, *267*, 17640−17648.

10.1021/ja070601r CCC: $37.00

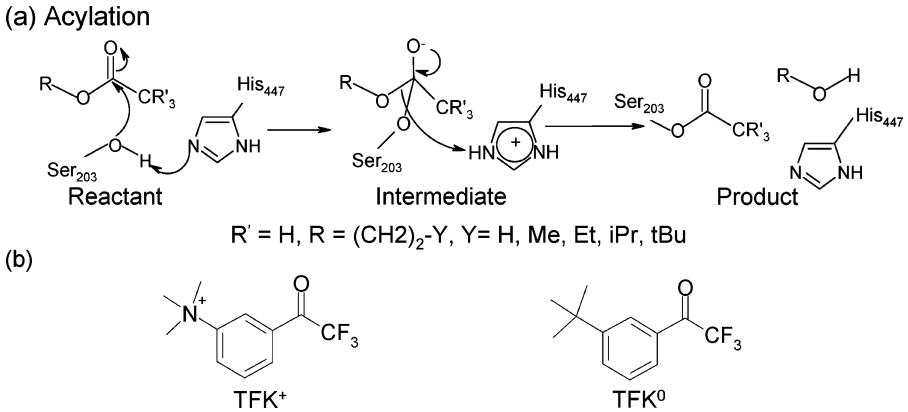

Figure 1. (a) Acylation mechanism in the wild-type AChE enzyme; (b) chemical structures of *TFK*$^+$ and *TFK*^{0}.

acylation reaction mechanism based on both experimental and theoretical explorations[16,17] is shown in Figure 1a. Ser203 and His447 are believed to be directly involved in the bond breaking and forming. Ser203 serves as a nucleophilic attacking site, and the imidazole group of His447 acts as a catalytic base which accepts one proton transferred from Ser203. However, for the third residue in the catalytic triad, Glu334, its detailed role remains elusive up to now.[18] In previous studies, in addition to maintaining the productive orientation of His447,[19] at least three different catalytic roles of Glu334 have been proposed. First, the "charge-relay" mechanism suggests that Glu334 functions as a catalytic base, which accepts one proton from the N_δ atom of His447;[20−22] the second is a "low-barrier hydrogen bond or short, strong hydrogen bond (LBHB or SSHB)" mechanism, originally proposed based on NMR studies,[23−26] in which a short hydrogen bond between O_δ of Glu334 and N_δ of His447 (<2.65 Å) is thought to supply 10−20 kcal/mol "resonance stabilization" to the transition state;[18,27−29] recent experimental and theoretical studies also pointed to a third possible mechanism, in which the electrostatic interaction between the carboxylate of Glu334 and the incipient imidazolium cation stabilizes the transition state and intermediate.[17,30−32] The proton is mostly localized on His447-N_δ, and hence it is not participating in a low-barrier hydrogen bond. When the proton hopping occurs, it has a destabilizing effect on the intermediate.[33,34]

Table 1. Rate Constants for Association and Dissociation of Inhibitors *TFK*$^+$ and *TFK*^{0} with Mouse AChEs Measured by Experiments[37,38] (Units of k_{on} and k_{off} are 10^9 M^{-1} min^{-1} and 10^{-3} min^{-1}, Respectively)

	wild-type mAChE		H447I mutant mAChE	
	k_{on}	k_{off}	k_{on}	k_{off}
TFK$^+$	980 ± 60	1.1 ± 0.3	~10[a]	~1.0[a]
TFK^0	2.2 ± 0.3	15 ± 1	*N*/*A*[b]	*N*/*A*[b]

[a] Unpublished data. [b] There is no apparent binding affinity detected.

However, recent experimental mutagenesis studies have brought new challenges to all the above proposed reaction mechanisms. *TFK*$^+$ (*m*-(*N*,*N*,*N*-trimethylammonio)trifluoroacetophenone (TMTFA)) (see Figure 1b), a common inhibitor to AChE, can still react with the mouse AChE (mAChE), even with the replacement of His447 by a hydrophobic Ile. In contrast, its neutral analogue, *TFK*^{0}, shows no apparent binding activity to H447I mutant, while it shows slightly reduced binding to the wild-type mAChE as compared to *TFK*$^+$ (see Table 1). Additionally, Ser229, which makes direct contact with the side chain of Glu334, is believed to be essential to maintaining the integrity of the catalytic triad; its critical importance for the enzymatic activity seems unique to the cholinesterases.[35] However, substitution of Ser229 with an Asn residue, at an equivalent position in Zebra fish AChE, yields a protein with no detectable catalytic activity.[36] So far, how Ser229 is involved in AChE acylation is still an open question.

In order to explore the enzymatic activity of H447I mutant mAChE, as well as the role of Ser229 in the acylation reaction, we have performed computational studies on both *TFK*$^+$ and *TFK*^{0} binding to the wild-type and H447I mutant mAChEs, using a combined *ab initio* quantum mechanical and molecular mechanical (QM/MM) approach, as well as multiple MD simulations. In our study, a water molecule is found to play an essential catalytic role in place of His447 in the binding reaction of *TFK*$^+$ to the H447I mutant. Along with this water molecule, Ser203 and Glu334 form a new stable catalytic triad. During reaction, Ser203 delivers a proton to the water molecule while the water molecule serves as a charge relayer to pass one proton to Glu334. The QM/MM free energy barrier for the reaction is lower than 8.0 kcal/mol. On the other hand, the water triad was unable to be retained in the corresponding *TFK*^{0}/H447I com-

(16) Quinn, D. M. *Chem. Rev.* **1987**, *87*, 955−979.
(17) Zhang, Y. K.; Kua, J.; McCammon, J. A. *J. Am. Chem. Soc.* **2002**, *124*, 10572−10577.
(18) Quinn, D.; Medhekar, R.; Baker, N. *Comprehensive Natural Products Chemistry: Enzymes, Enzyme Mechanisms, Proteins, and Aspects of NO Chemistry*; Elsevier Science: Oxford, U.K., 1999.
(19) Dodson, G.; Wlodawer, A. *Trends Biochem. Sci.* **1998**, *23*, 347−352.
(20) Blow, D. M.; Birktoft, J. J.; Hartley, B. S. *Nature* **1969**, *221*, 337−340.
(21) Bachovchin, W. W.; Roberts, J. D. *J. Am. Chem. Soc.* **1978**, *100*, 8041−8047.
(22) Tachikawa, H.; Igarashi, M.; Nishihira, J.; Ishibashi, T. *J. Photochem. Photobiol., B* **2005**, *79*, 11−23.
(23) Gerlt, J. A.; Gassman, P. G. *J. Am. Chem. Soc.* **1993**, *115*, 11552−11568.
(24) Gerlt, J. A.; Gassman, P. G. *Biochemistry* **1993**, *32*, 11943−11952.
(25) Cleland, W. W.; Kreevoy, M. M. *Science* **1994**, *264*, 1887−1890.
(26) Frey, P. A.; Whitt, S. A.; Tobin, J. B. *Science* **1994**, *264*, 1927−1930.
(27) Massiah, M. A.; Viragh, C.; Reddy, P. M.; Kovach, I. M.; Johnson, J.; Rosenberry, T. L.; Mildvan, A. S. *Biochemistry* **2001**, *40*, 5682−5690.
(28) Stranzl, G. R.; Gruber, K.; Steinkellner, G.; Zangger, K.; Schwab, H.; Kratky, C. *J. Biol. Chem.* **2004**, *279*, 3699−3707.
(29) Zhao, L.; Liao, H.; Tsai, M. D. *J. Biol. Chem.* **2004**, *279*, 31995−32000.
(30) Warshel, A.; Narayszabo, G.; Sussman, F.; Hwang, J. K. *Biochemistry* **1989**, *28*, 3629−3637.
(31) Fuxreiter, M.; Warshel, A. *J. Am. Chem. Soc.* **1998**, *120*, 183−194.
(32) Katona, G.; Wilmouth, R. C.; Wright, P. A.; Berglund, G. I.; Hajdu, J.; Neutze, R.; Schofield, C. J. *J. Biol. Chem.* **2002**, *277*, 21962−21970.
(33) Topf, M.; Varnai, P.; Richards, W. G. *J. Am. Chem. Soc.* **2002**, *124*, 14780−14788.
(34) Ishida, T. *Biochemistry* **2006**, *45*, 5413−5420.
(35) Shafferman, A.; Barak, D.; Kaplan, D.; Ordentlich, A.; Kronman, C.; Velan, B. *Chem.-Biol. Interact.* **2005**, *157*, 123−131.
(36) Behra, M.; Cousin, X.; Bertrand, C.; Vonesch, J. L.; Biellmann, D.; Chatonnet, A.; Strahle, U. *Nat. Neurosci.* **2002**, *5*, 111−118.

plexes from multiple MD simulations, indicating that TFK^0 might not be able to stably bind to the H447I mutant. To further validate our QM/MM calculations, we also used thermodynamic integration (TI) calculations to investigate the binding energy differences between TFK^0 and TFK^+ in both the wild-type and H447 mutant enzymes. The TI calculations also suggest that the binding of TFK^+ to both enzymes is much stronger than the neutral analogue TFK^0, which is consistent with experimental observations as well as the above QM/MM calculations.

2. Computational Methods

2.1. Construction of Wild-Type Complex Models. Our starting point is the X-ray structure of AChE-TFK^+ complex (PDB code: 2H9Y),[39] in which a covalent bond is formed between TFK^+ and Ser203-O_γ (denoted as the [W−T^+] model[40]). Missing hydrogen atoms for the protein were added via InsightII,[41] while hydrogens for conserved crystal waters were added and optimized by WHATIF.[42] For histidine residues, calculations of the local electrostatic microenvironment and the effective pK_a with WHATIF indicated that His447 should be protonated on both N_ϵ and N_δ, while the others are neutral residues: HID381, HID387, HID405 with N_δ protonated; HIE212, HIE223, HIE284, HIE287, HIE393, HIE432 with N_ϵ protonated. The [W−T^0] model was obtained by manually modifying TFK^+ to its neutral analogue TFK^0. The atomic charges for both TFK^+ and TFK^0 as well as Ser-TFK^+ and Ser-TFK^0 were derived by fitting to HF/6-31G* electrostatic potentials (ESP) using the RESP module. Other force parameters for TFK^+ and TFK^0 were adapted from the standard force field by following the general parametrization procedures outlined in the AMBER manual.[43,44]

After relaxing the added atoms in the gas phase, each structure was immersed in a cubic TIP3P water box and neutralized by addition of Na^+ counterions using the AMBER Leap module. This led to the [W−T^+] simulation system of 70 017 atoms and [W−T^0] simulation system of 72 598 atoms, respectively. MD simulations were conducted in the NPT ensemble at 300 K and 1 atm. The SHAKE algorithm[45] was used to constrain all bond lengths involving hydrogens. A 10.0 Å cutoff was used for nonbonded interactions; the neighbor pair list was updated every 10 steps. The long-range electrostatic interactions were treated with the Particle Mesh Ewald method.[46] The two prepared systems were first equilibrated with a series of minimizations interspersed by short MD simulations, and then extended to 10 ns MD simulations.

In each MD simulation trajectory, two snapshots, one from the first 1 ns and one from the last 1 ns, were selected for the following QM/MM investigations. These selected structures were first minimized using the MM method and then optimized with the B3LYP(6-31G*) QM/MM calculations using an iterative minimization approach,[47] finally leading to four [W−T^+] and [W−T^0] structures.

2.2. Construction of H447I Mutant Complex Models. Since there is no crystal structure of the H447I mutant so far, we tried two approaches to prepare the initial noncovalent complex structure of H447I and TFK^+ (denoted as the [M·T^+] model). The first approach is to use the multiple docking approach introduced by Kua et al.[48] His447 in the apo mAChE crystal structure (PDB code: 1J06) was manually modified to Ile, and then TFK^+ was docked into 1000 snapshots evenly chosen from the last 1 ns trajectory of a 10 ns apo H447I mutant MD simulation. The Autodock 3.0 program[49] was used for all the docking studies. The search method used was the Lamarckian genetic algorithm (LGA) set at level 2 with the top six structures reported. Finally, according to the criteria suggested in Kua et al.,[48] the best six complex structures were selected and immersed into explicit water boxes, and subsequent MD simulations were set up to relax each system. To prevent TFK^+ dislocation from the esteratic binding site, a 20.0 kcal/(mol·Å^2) harmonic restraint between the carbonyl-C of TFK^+ and Ser203-O_γ was applied during simulations. The second approach is to start from the noncovalent [W·T^+] structure obtained from our QM/MM calculations of the wild-type enzyme with TFK^+ (see below for details) and then manually replace HID447 (Note: The N_ϵ proton originally in the [W−T^+] complex is transferred to Ser203 in the [W·T^+] model after the QM/MM run) with Ile. Another MD simulation of the resulting system was then set up by following the same procedure as outlined in the first approach. The total number of atoms in these seven MD simulations is around 70 000−75 000. Similarly, seven initial models of H447I and TFK^0 ([M·T^0]) were obtained with the same procedure. Additionally, an eighth [M·T^0] model was obtained by directly modifying TFK^+ to TFK^0 in one of the [M·T^+] models. Therefore, a total of eight [M·T^0] models were prepared and subjected to further theoretical investigations.

2.3. QM/MM Free Energy Calculations. The pseudobond *ab initio* QM/MM approach[47,50] has achieved great success in accurate modeling of the chemistry at an enzyme active site while properly including the effects of the enzymatic environment. It has been applied to various enzyme reactions, including enolase,[51] acetylcholinesterase,[17] 4-oxalocrotonate tautomerase,[52] kinase,[53] and methyltransferase.[54] Free energies along the reaction coordinates can be determined by free energy perturbation (FEP) calculations with the harmonic approximation.[47,55] The effect of enzyme dynamics can be taken into account by using the ensemble of enzyme−substrate complex structures sampled from an MD simulation as initial structures for QM/MM calculations.[54,56,57]

The QM/MM approach divides the whole enzyme−substrate system into a QM and an MM subsystem. The active site of the enzyme was described by a QM Hamiltonian, and the influence of the remainders of the protein and the solvent was included via a coupled MM potential. The code combining the modified Gaussian 98[58] and Tinker 3.6[59] was utilized for all the calculations. With the reaction coordinate driving (RCD) method, an efficient iterative restrained optimization procedure[47] was repeatedly applied to all the chosen points along the reaction

(37) Radić, Z.; Quinn, D. M.; McCammon, J. A.; Taylor, P. *J. Biol. Chem.* **1997**, *272*, 23265−23277.
(38) Radić, Z.; Taylor, P. *J. Biol. Chem.* **2001**, *276*, 4622−4633.
(39) Bourne, Y.; Radić, Z.; Sulzenbacher, G.; Kim, E.; Taylor, P.; Marchot, P. *J. Biol. Chem.* **2006**, *281*, 29256−29267.
(40) "*W*", "*M*", "T^+", and "T^0" represent the wild-type mAChE, H447I mutant, TFK^+, and TFK^0, respectively; [X−Y] and [X·Y] represent the covalent and noncovalent complexes of the X enzyme and Y ligand, respectively.
(41) *InsightII*, version 2000.1; Accelrys Software Inc.: San Diego, CA, 2000.
(42) Vriend, G. *J. Mol. Graphics* **1990**, *8*, 52−56.
(43) Cornell, W. D.; Cieplak, P.; Bayly, C. I.; Gould, I. R.; Merz, K. M.; Ferguson, D. M.; Spellmeyer, D. C.; Fox, T.; Caldwell, J. W.; Kollman, P. A. *J. Am. Chem. Soc.* **1995**, *117*, 5179−5197.
(44) Case, D., et al. *Amber 8.0*; University of California, San Francisco, CA, 2004.
(45) Ryckaert, J. P.; Ciccotti, G.; Berendsen, H. J. C. *J. Comput. Phys.* **1977**, *23*, 327−341.
(46) Darden, T.; York, D.; Pedersen, L. *J. Chem. Phys.* **1993**, *98*, 10089−10092.
(47) Zhang, Y. K.; Liu, H. Y.; Yang, W. T. *J. Chem. Phys.* **2000**, *112*, 3483−3492.
(48) Kua, J.; Zhang, Y. K.; McCammon, J. A. *J. Am. Chem. Soc.* **2002**, *124*, 8260−8267.
(49) Morris, G. M.; Goodsell, D. S.; Halliday, R. S.; Huey, R.; Hart, W. E.; Belew, R. K.; Olson, A. J. *J. Comput. Chem.* **1998**, *19*, 1639−1662.
(50) Zhang, Y. K.; Lee, T. S.; Yang, W. T. *J. Chem. Phys.* **1999**, *110*, 46−54.
(51) Liu, H. Y.; Zhang, Y. K.; Yang, W. T. *J. Am. Chem. Soc.* **2000**, *122*, 6560−6570.
(52) Cisneros, G. A.; Wang, M.; Silinski, P.; Fitzgerald, M. C.; Yang, W. T. *Biochemistry* **2004**, *43*, 6885−6892.
(53) Cheng, Y. H.; Zhang, Y. K.; McCammon, J. A. *J. Am. Chem. Soc.* **2005**, *127*, 1553−1562.
(54) Hu, P.; Zhang, Y. K. *J. Am. Chem. Soc.* **2006**, *128*, 1272−1278.
(55) Zhang, Y.; Liu, H.; Yang, W. Ab Initio QM/MM and Free Energy Calculations of Enzyme Reactions. In *Methods for Macromolecular Modeling*; Schlick, T., et al., Eds.; Springer-Verlag: New York, 2002.
(56) Zhang, Y. K.; Kua, J.; McCammon, J. A. *J. Phys. Chem. B* **2003**, *107*, 4459−4463.
(57) Cheng, Y. H.; Zhang, Y. K.; McCammon, J. A. *Protein Sci.* **2006**, *15*, 672−683.
(58) Frisch, M. J., et al. *Gaussian 98*, revision A.5; Gaussian, Inc.: Pittsburgh, PA, 1998.
(59) Ponder, J. W. *TINKER, Software Tools for Molecular Design*, version 3.6; The most updated version for the TINKER program can be obtained from J. W. Ponder's World Wide Web site at http://dasher.wustl.edu/tinker., February 1998.

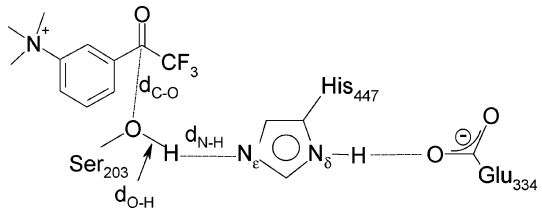

Figure 2. Illustration of the reaction coordinate $d_{C-O} + d_{N-H} - d_{O-H}$ selected for the reverse reaction of TFK^+ (or TFK^0) binding.

Table 2. Calculated TFK^+ and TFK^0 Binding Free Energies through Thermodynamic Integration (Unit is kcal/mol)

	ΔA^{H_2O}	$\Delta A^{E}_{noncovalent}$	$\Delta A^{E}_{covalent}$	$\Delta\Delta A^{Diffusion}$	$\Delta\Delta A^{Reaction}$
wild-type	37.9	48.4	58.1	10.5	9.7
H447I mutant	37.9	45.7	66.6[a]	7.8	20.9[a]
Δ(H447I − wild)	0.0	−2.7	8.5	**−2.7**	**11.2**

[a] Suppose the TFK^0/H447I complex exists.

coordinate, resulting in a minimum energy path. For each identified stationary point, the large MM subsystem was relaxed with the truncated Newton method in Cartesian coordinates, while the small QM subsystem was treated using the quasi-Newton minimizer at the B3LYP/6-31G* level in redundant internal coordinates, and the corresponding vibrational frequencies were determined. The contribution of the QM subsystem fluctuation to free energy change was then calculated with the obtained frequencies using a harmonic approximation. Finally, the free energy changes associated with QM/MM interactions along the reaction path were determined by FEP calculations. In FEP calculations, sampling of the MM subsystem was carried out with the QM subsystem frozen at different states along the reaction path. The total free energy difference between any two points A and B along the reaction coordinate was obtained by adding up the contributions of the QM subsystem energy difference $\Delta E_{qm}(A \rightarrow B)$, the QM fluctuation to the free energy difference $\Delta F^{fluc}_{qm}(A \rightarrow B)$, and the free energy change associated with the QM/MM interaction $\Delta F_{qm/mm}(A \rightarrow B)$.[47,54]

For the QM/MM calculations on the [W−T$^+$] and [W−T^0] models, the QM subsystem consists of the side chain of Ser-TFK$^+$ (or Ser-TFK^0), and HIP447 (both N_ϵ and N_δ are protonated) and Glu334, resulting in a total of 57 QM atoms. The boundary between the QM and MM subsystems was treated using the pseudobond approach.[50] All other atoms are described by the classical MM force fields. Similarly to the ACh-mAChE acylation QM/MM calculation,[17,56] the reaction coordinate was chosen to be $d_{C-O} + d_{N-H} - d_{O-H}$ that represents simultaneous bond breaking of carbonyl-C in Ser-TFK$^+$ (or Ser-TFK^0) and seryl O_γ and a bond forming between Ser203 and His447, as illustrated in Figure 2. The noncovalent Michaelis complex, which is denoted as [$W{\cdot}T^+$] or [$W{\cdot}T^0$], was obtained by running a reverse reaction starting from the corresponding [W−T$^+$] or [W−T^0].

Since our interest was the acylation reaction mechanism, only those atoms within 20.0 Å of the hydroxyl oxygen atom of Ser203 were allowed to move. No cutoff for nonbonded interactions was used in the QM/MM calculations. Throughout the calculations, the pseudobond was treated with the 6-31G* basis set and its corresponding effective core potential parameters.[50] AMBER 95 all-atom force field[43] and the TIP3P model for water[60] were used. In QM/MM-FE calculations, the time step used was 2 fs, and bond lengths involving hydrogen atoms were constrained. A twin-range cutoff method was used to treat nonbonded interactions, with a long-range cutoff of 12 Å, a short-range cutoff of 8 Å, and the nonbonded pair list updated every 20 steps. The temperature was maintained at 300 K using the weak coupling method with a coupling time of 0.1 ps. Each FEP calculation consisted of 50 ps of equilibration and 200 ps of sampling. The final relative free

(60) Jorgensen, W. L.; Chandrasekhar, J.; Madura, J. D.; Impey, R. W.; Klein, M. L. *J. Chem. Phys.* **1983**, *79*, 926−935.

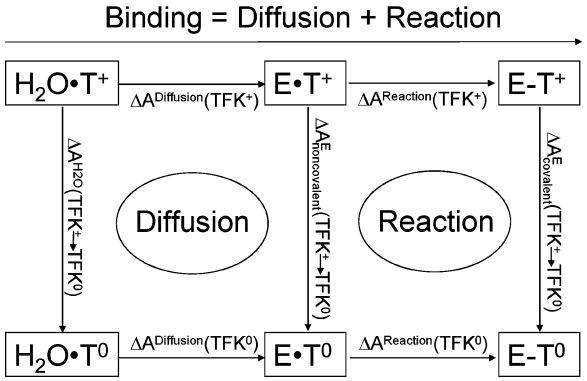

Figure 3. Thermodynamic cycle of TFK^+ and TFK^0 bindings in the mAChE. Here [$E{\cdot}T^+$] and [$E{\cdot}T^0$] refer to the noncovalent enzyme−ligand complexes, while [$E{-}T^+$] and [$E{-}T^0$] refer to the covalent complexes. "E" can represent either "W" (wild-type mAChE) or "M" (H447I mutant mAChE).

energies were taken as the average of the "forward" and "backward" perturbation results.

2.4. Thermodynamic Integration. To compare the binding free energy difference of TFK^+ and TFK^0 in the mAChE enzyme, we designed the "alchemical" thermodynamic cycle shown in Figure 3.

By Hess's law, we have

$$\Delta\Delta A^{Diffusion/Reaction}_{TFK^+\rightarrow TFK^0} = \Delta A^{Diffusion/Reaction}_{TFK^0} - \Delta A^{Diffusion/Reaction}_{TFK^+}$$
$$= \begin{cases} \Delta A^{E,noncovalent}_{TFK^+\rightarrow TFK^0} - \Delta A^{H_2O}_{TFK^+\rightarrow TFK^0} & Diffusion \\ \Delta A^{E,covalent}_{TFK^+\rightarrow TFK^0} - \Delta A^{E,noncovalent}_{TFK^+\rightarrow TFK^0} & Reaction \end{cases} \quad (2)$$

The potential energy of the system is expressed as a function of a coupling parameter λ that describes the transformation from TFK^+ to TFK^0; i.e.,

$$U(r,\lambda) = U_0(r) + \lambda U_{TFK^0}(r) + (1-\lambda)U_{TFK^+}(r) \quad (3)$$

with $\lambda = 0$ corresponding to a system with TFK^+ and $\lambda = 1$ corresponding to a system with TFK^0. $U_{TFK^0}(r)$ is the Hamiltonian of TFK^0, $U_{TFK^+}(r)$, the Hamiltonian of TFK^+, and $U_0(r)$, the Hamiltonian of the remainder of the system.

Then the free energy difference between $\lambda = 0$ (TFK^+) and $\lambda = 1$ (TFK^0) is

$$\Delta A_{\lambda=0\rightarrow 1} = \int_0^1 \left\langle \frac{\partial U(r,\lambda)}{\partial \lambda} \right\rangle_\lambda d\lambda \approx \sum_{i=1}^{n} w_i \langle \partial U(r,\lambda)/\partial\lambda \rangle_{\lambda_i} \quad (4)$$

The TI calculations were performed by using the AMBER 8.0 package. Two thermodynamic cycles are calculated, one corresponding to the diffusion stage and the other corresponding to the reaction stage. For each calculation, a set of 12 λ values were used with λ = 0.009 22, 0.047 94, 0.115 05, 0.206 34, 0.316 08, 0.437 38, 0.562 62, 0.683 92, 0.793 66, 0.884 95, 0.952 06, 0.990 78, respectively. For each λ, the system was equilibrated for 40 ps at 300 K and data were collected for the subsequent 100 ps. The convergence of the simulation was monitored by checking the forward and backward calculations.

3. Results and Discussions

3.1. Wild-Type mAChE Complexes. Figure 4 illustrates the calculated QM/MM potential energy paths for both TFK^+ and TFK^0 binding to the wild-type mAChE. Both binding processes are spontaneous, and there appears no apparent energy barrier associated with the nucleophilic attack of Ser203-O_γ at the carbonyl-C of the ligand. The potential energy at the B3LYP-(6-31G*) QM/MM level monotonically drops ∼19.3 kcal/mol during the covalent bond forming between Ser203-O_γ and the

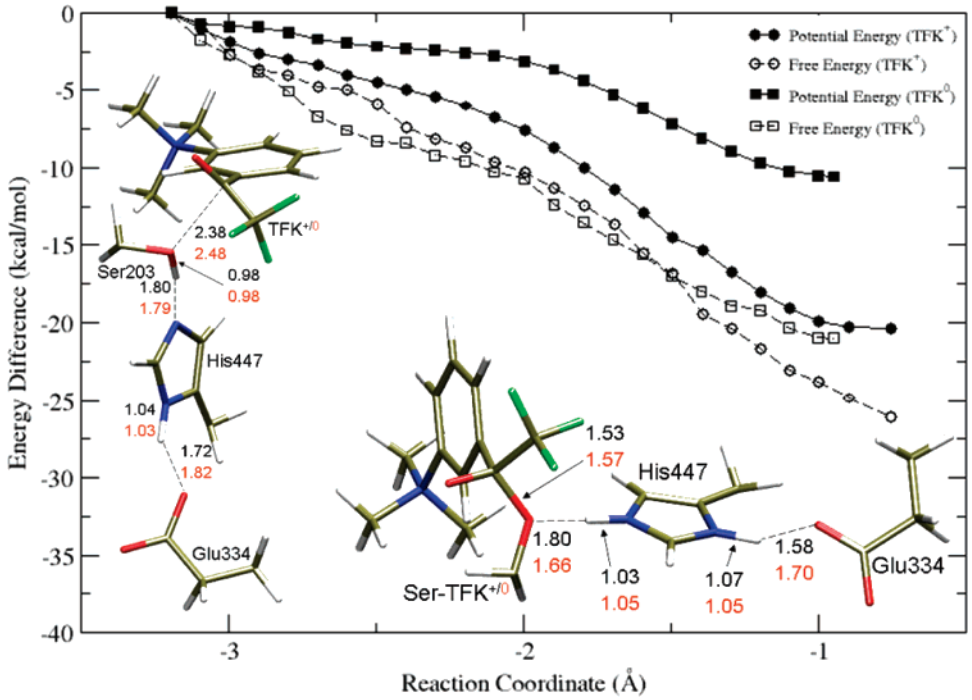

Figure 4. Determined minimum-energy paths and corresponding free energy changes along the reaction coordinate for the *TFK*$^+$ and *TFK*^{0} binding to the wild-type mAChE. From left to right, the reaction proceeds from the reactant to the tetrahedral product without an activation barrier. The values in black and red denote the bond lengths of the *TFK*$^+$ and *TFK*^{0} cases, respectively.

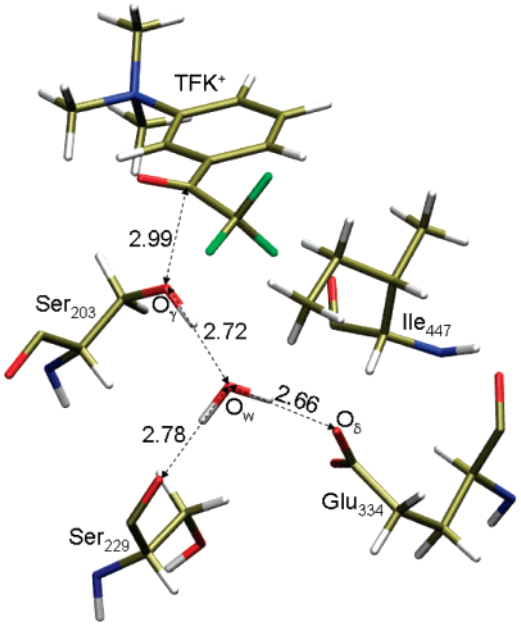

Figure 5. "Water" triad in the active site of the six [*M*·*T*$^+$] models. The values of the distances in Å are averaged among six models.

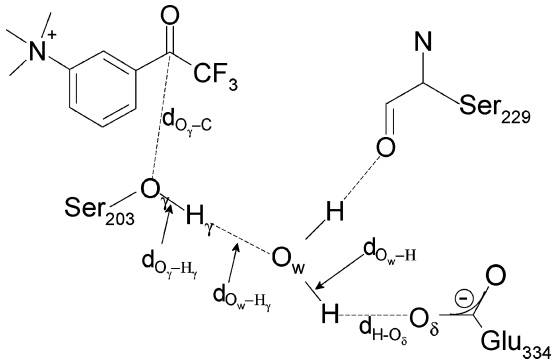

Figure 6. Illustration of the reaction coordinate used for the H447I mutant and *TFK*$^+$ reaction, which is $d_{O_\gamma-H_\gamma} + d_{O_w-H} - d_{O_\gamma-C} - d_{O_w-H_\gamma} - d_{H-O_\delta}$.

carbonyl-C of *TFK*$^+$, while only a 10.6 kcal/mol decrease is observed between mAChE and *TFK*^{0}. To estimate the free energy change of the acylation reaction, we carried out a QM/MM-FE perturbation study on both reactions of *TFK*$^+$ and *TFK*^{0} with mAChE; results are shown in Figure 4. The free energy differences between the reactant and product are 26.1 and 21.0 kcal/mol for *TFK*$^+$ and *TFK*^{0}, respectively, indicating that the covalent rearrangements associated with the binding of both inhibitors are favorable.

Additionally, two thermodynamic cycles as shown in Figure 3 were designed to compare the binding affinity difference of *TFK*$^+$ and *TFK*^{0} in the same mAChE target. As shown in Table 2, it turns out that the free energy differences between *TFK*$^+$ and *TFK*^{0} are 10.5 kcal/mol at the diffusion stage (forming an initial noncovalent complex) and 9.7 kcal/mol at the reaction stage (forming a covalent complex). Since the reaction is spontaneous without any barrier, the diffusion stage is rate-determined. Our result at the diffusion stage is qualitatively consistent with experimental measurements that the ratio of k_{on} and k_{off} with *TFK*$^+$ is ∼4 orders of magnitude larger than that of *TFK*^{0},[37,38] while the reaction free energy differences of 9.7 kcal/mol derived from the thermodynamic integration is in good agreement with that from QM/MM calculations. The detailed calculations were shown in the Supporting Information.

3.2. Complex of H447I Mutant and *TFK*$^+$. As mentioned in the Computational Methods section, seven noncovalent complex [*M*·*T*$^+$] models of the H447I mutant and *TFK*$^+$ were obtained via docking and QM/MM calculations. During the subsequent MD simulations of these models, in six of seven models, a water molecule was observed to diffuse into the center of the triangle formed by Ser203, Ser229, and Glu334 in the

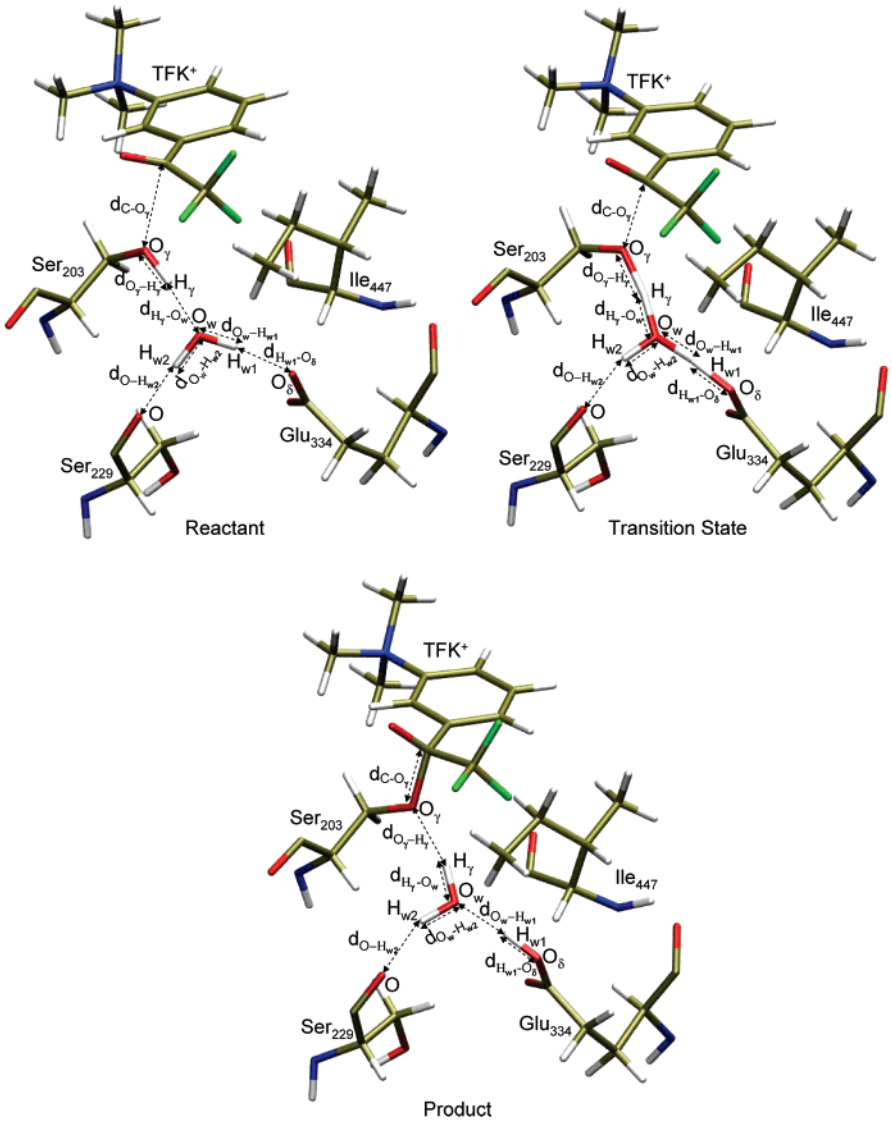

Figure 7. Active sites of the reactant, transition state, and product in QM/MM calculations for the complex of H447I mutant and TFK^+.

first 2 ns simulations; a representative snapshot from the simulation is shown in Figure 5. Then we extended our MD simulations to 10 ns for each model. The average distance of the hydroxyl oxygen O_γ of Ser203 to the oxygen O_w of the water is 2.72 ± 0.12 Å, that of the carboxyl oxygen of the Ser229 backbone to O_w of the water is 2.78 ± 0.18 Å, and that of O_w of the water to one of carboxyl oxygens $O_{\delta 1}$ of Glu334 is 2.66 ± 0.12 Å in all of the 10 ns trajectories. Generally, an effective hydrogen bond can be characterized by the short distance between the heteroatoms (less than 3.50 Å) and a bond angle greater than 135°.[44,61,62] Using this criteria, the hydrogen bond between the Ser203 O_γ and O_w is found in all the structures in the 10 ns simulations, while the hydrogen bond between O_w and $O_{\delta 1}$ is ~99% and that between O_w and Ser229-O is ~95%. The water molecule is observed to flip between Ser229-O and $O_{\delta 1}$, while the hydrogen bond between O_γ and O_w stays stable.

Three snapshots from the above MD simulations were selected to explore the acylation reaction mechanism in the H447I mutant. The water molecules beyond a 27 Å solvent water sphere, centered on the active site (the hydroxyl oxygen O_γ of Ser203), were removed. The three prepared QM/MM models have 10 059 atoms (562 water molecules), 10 176 atoms (602 water molecules), and 10 170 atoms (600 water molecules), respectively. Each snapshot was first relaxed by the MM method and then optimized with B3LYP(6-31G*) QM/MM calculations using an iterative minimization approach,[47] leading to an optimized structure for the reactant. The QM subsystem consists of the sidechains of Ser203 and Glu334, the water bridge and TFK^+, with the broken $C_\beta - C_\alpha$ bonds of Ser203 and Glu334 treated as two pseudobonds,[50] resulting in a total of 48 QM atoms. All other atoms are treated by MM. The reaction coordinate (RC) is shown in Figure 6. Both forward and backward RC driving calculations yield consistent curves, and all the reaction paths are smooth and continuous.

All three QM/MM calculations led to very consistent results, in which the water molecule between Ser203 and Glu334 plays a "charge-relay" role during the TFK^+ binding reaction with the H447I mutant. Table 3 presents the relative potential energies in the reactant (noncovalent complex), transition state, and

(61) Eriksson, M. A. L.; Nilsson, L. *Eur. Biophys. J. Biophys. Lett.* **1999**, *28*, 102−111.
(62) Sheu, S. Y.; Yang, D. Y.; Selzle, H. L.; Schlag, E. W. Energetics of hydrogen bonds in peptides. *Proc. Natl. Acad. Sci. U.S.A.* **2003**, *100* (22).

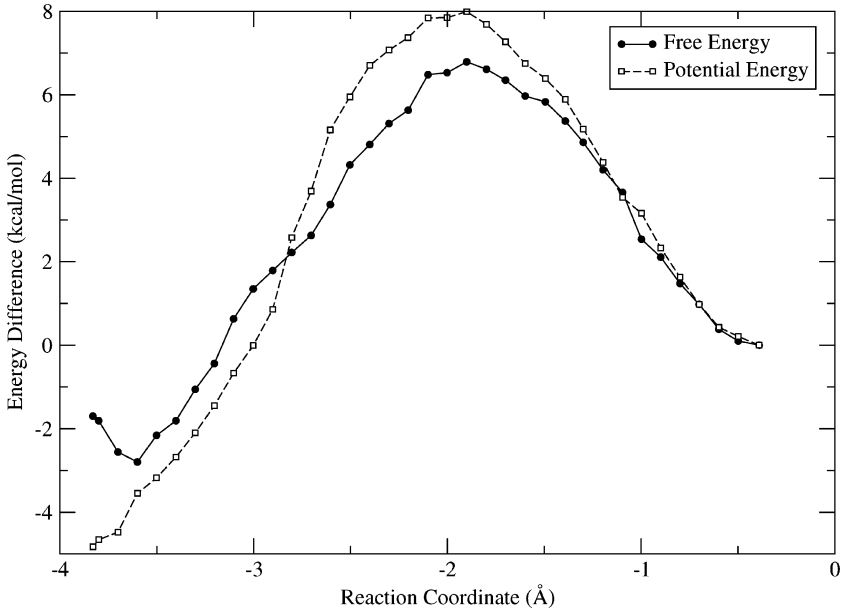

Figure 8. Free energy and potential energy paths of the acylation reaction along the reaction coordinate in one of the three [$M{\cdot}T^+$] models.

Table 3. Calculated QM/MM Potential Energy Differences (kcal/mol) for Three QM/MM Models[a]

	MP2(6-31+G*)/MM	B3LYP(6-31+G*)/MM	B3LYP(6-31G*)/MM
	First Snapshot		
reactant	0.0	0.0	0.0
transition state	8.2	7.4	8.2
product	−5.0	−1.1	2.0
	Second Snapshot		
reactant	0.0	0.0	0.0
transition state	4.2	5.8	7.5
product	−8.0	−2.5	0.0
	Third Snapshot		
reactant	0.0	0.0	0.0
transition state	10.6	10.3	10.4
product	0.4	3.8	4.4

[a] The geometries are relaxed at the B3LYP(6-31G*)/MM level, and then single-point calculations are performed at three different levels.

Table 4. Key Bond Lengths in the Reaction Centers of the Reactant, Transition State, and Product in the QM/MM Calculations of [$M{\cdot}T^+$] Models

	d_{C-O_γ}	$d_{O_\gamma-H_\gamma}$	$d_{H_\gamma-O_w}$	$d_{O_w-H_{w1}}$	$d_{H_{w1}-O_\delta}$	$d_{O_w-H_{w2}}$	$d_{O-H_{w2}}$
	First Snapshot						
reactant	2.48	1.01	1.65	0.98	1.71	0.98	1.71
transition state	2.03	1.29	1.16	1.17	1.27	0.98	1.75
product	1.60	1.81	0.99	1.66	1.01	0.98	1.80
	Second Snapshot						
reactant	2.72	1.01	1.67	1.01	1.63	0.98	1.89
transition state	1.92	1.28	1.16	1.12	1.32	0.98	2.18
product	1.58	1.79	0.99	1.66	1.02	0.98	2.29
	Third Snapshot						
reactant	2.58	1.01	1.63	1.01	1.64	0.97	1.83
transition state	2.00	1.29	1.15	1.19	1.24	0.98	1.90
product	1.64	1.69	0.99	1.58	1.02	0.98	1.91

product (covalent complex), respectively. The calculated potential energy barriers at the MP2(6-31+G*)/MM level are 8.2, 4.2, 10.6 kcal/mol. Several key geometry elements in the reactant, transition state, and product are shown in Figure 7 and also listed in Table 4. In spite of several variations in the three initial setups, the active site structures of the transition state and product are quite similar in the three calculations.

To estimate the free energy change of the acylation reaction in H447I mutant, we carried out a QM/MM-FE perturbation study on all the three snapshots. Figure 8 depicts one of three free energy pathways, along with the corresponding potential energy path. The dynamic fluctuations of MM residues contribute at least 2 kcal/mol to the decrease of the reaction barrier.

In order to quantitatively assess the role of the individual residues in the TFK^+ binding reaction, we also calculated the Van der Waals and electrostatic interactions between each MM residue and QM subsystem for both the transition state and reactant. The structures were taken from our B3LYP(6-31G*)/MM calculations, and the partial charges were determined by the single-point calculations for the transition state and reactant structures, respectively. The energy difference between the transition state and reactant is taken as the individual barrier contribution of each MM residue. All the main contributors and their average contributions are listed in Table 5.

In accord with experimental findings, our calculations show that the oxyanion hole (Gly121, Gly122, Ala204) plays an important role in stabilizing the transition state. The reactivities of both G121A and G122A mutants toward TFK^+ were 2000−11 000-fold lower than that of the wild-type AChE.[63] G121A only affected the turnover number, and mutation of Gly122 also had an effect on the Michaelis constant[63] for substrate acetylthiocholine hydrolysis. In our 10 ns MD simulations, only the backbone nitrogens of Gly122 and Ala204 form stable hydrogen bonds with the carbonyl oxygen of TFK^+, which might help to optimize the substrate orientation to participate in the acylation reaction. The total stabilization energy contributed by the oxyanion hole is around 7.0 kcal/mol. In addition, Gly120 in the H447I mutant seems to destabilize the transition state, which is different from what is seen in the wild-type AChE.[17] In all three QM/MM calculations, Glu202 occupies a position similar to that in the wild-type and contributes around 3−7 kcal/mol destabilization to the transition state, consistent with previous theoretical results.[17] In our MD simulations, Glu202 is found

(63) Ordentlich, A.; Barak, D.; Kronman, C.; Ariel, N.; Segall, Y.; Velan, B.; Shafferman, A. *J. Biol. Chem.* **1998**, *273*, 19509−19517.

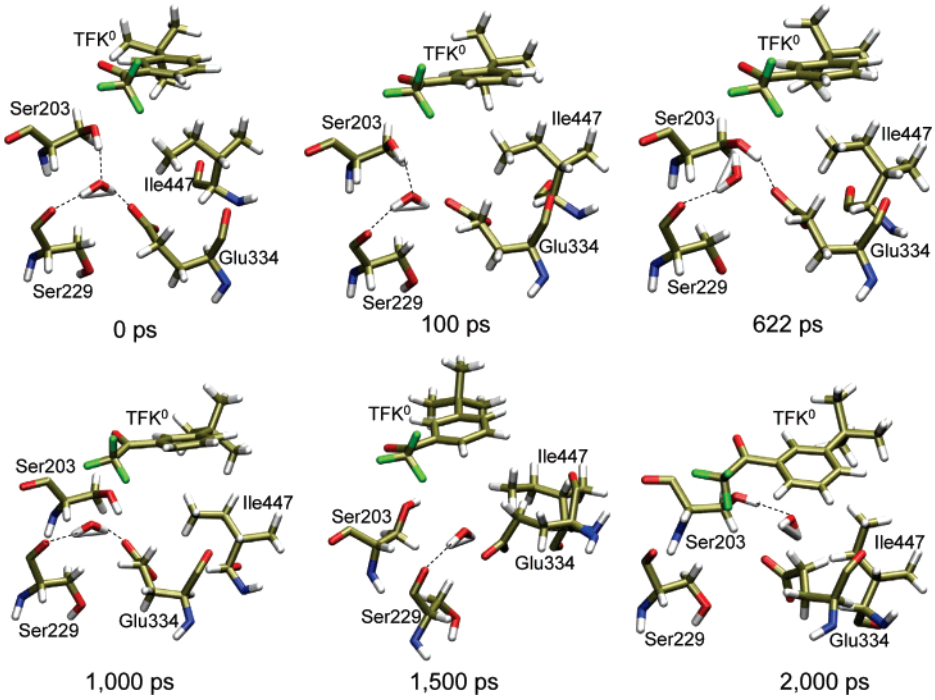

Figure 9. Several key residue elements in the active center of the complex of H447I mutant and TFK^0 during one of the MD simulations.

Table 5. Individual Residue Contributions to the Transition State Stabilization or Destabilization for Three H447I Mutant Snapshots (Calculation Based on MP2(6-31+G*)/MM Calculations)[a]

	$E_{ele+vdw}$		
	first snapshot	second snapshot	third snapshot
Asp74	1.3	1.2	2.1
Gly120	1.7	2.1	5.7
Gly121	−1.9	−8.3	−1.9
Gly122	−1.9	−2.6	−2.5
Glu202	6.1	3.0	3.7
Ala204	−2.2	−3.5	−2.5
Glu285	1.7	1.4	1.4
Lys332	2.4	1.9	2.2
Asp333	−3.1	−2.2	−2.9
Asp396	−2.1	−1.7	−2.0
Asp404	−3.2	−2.3	−2.2
Glu431	−1.6	−1.2	−1.7
Ile447	2.8	1.6	3.5
Gly448	2.1	1.8	3.9
Glu450	−2.0	−2.0	−2.1
Arg525	2.2	1.7	1.8

[a] $E_{ele+vdw}$ refers to the total nonbonded interaction energy including electrostatic and vdW parts. Energy units are in kcal/mol.

to play an important role in maintaining the overall structure of the active center. A hydrogen-bond networked cluster of polar residues, including Tyr133, Glu202, Glu450, Ser229, and two water molecules (one is between Tyr133 and Glu202, and the other is between Glu450 and Glu202) are lined on one side of the catalytic triad. Although Ser229 does not directly participate in bond breaking and forming, it plays an essential role in maintaining the integrity of the active site at both the wild-type and H447I mutant mAChEs. The enzyme loses its activity without Ser229.[64] Finally, it must be noted that the hydrophobic Ile447 is not directly involved in the bond breaking and forming but contributes 3 to 4 kcal/mol destabilization energy to the transition state.

(64) Stok, J. E.; Goloshchapov, A.; Song, C.; Wheelock, C. E.; Derbel, M. B. H.; Morisseau, C.; Hammock, B. D. *Arch. Biochem. Biophys.* **2004**, *430*, 247−255.

3.3. Complex of H447I Mutant and TFK^0. As mentioned in the Computational Methods section, a total of eight [$M{\cdot}T^0$] complex models were obtained through three different approaches. The resulting eight models were then subjected to 10 ns MD simulations. Unlike in the [$M{\cdot}T^+$] models, none of these [$M{\cdot}T^0$] models formed a stable "water triad" during the simulations. Even when the simulation started from a model based on [$M{\cdot}T^+$] (the third approach for generating the [$M{\cdot}T^0$] model as outlined in the Computational Methods section), in which the "water triad'' has been formed, the water inside the Ser203, Ser229, and Glu334 departed in less than 1 ns of MD simulation. Figure 9 displays the positions of several key active site residues during one of the MD simulations. In all these simulations, the hydrogen bond between Ser203 and the water was either disrupted after the first 2 ns of simulation or never formed. Therefore, in the [$M{\cdot}T^0$] models, we failed to find any stable catalytic base that can accept a proton from Ser203 during the acylation reaction, which is consistent with experimental observations that TFK^0 shows no activity in the H447I mutant. Additionally, QM/MM calculation with the initial structure of [$M{\cdot}T^0$] directly modified from [$M{\cdot}T^+$] failed to reach a convergence during optimization. All these facts indicate that the positive charge of the ligand TFK^+ plays an essential role in forming an appropriate active center conformation for the H447I mutant binding reaction. The positive charge might help to stabilize the negatively charged residues Glu202 and Glu334, as well as the oxyanion hole, which might have H-bonding with Ser203 and Ser229. Once the catalytic water diffuses into the center of the catalytic triangle, the triangle is "locked" and keeps very stable. However, the "lock" can be broken easily or even never formed if TFK^+ is replaced by TFK^0 as shown in Figure 9. As compared to TFK^+, larger RMSDs for TFK^0 have been captured in MD simulations.

Furthermore, our TI calculation also confirms that thermodynamically the TFK^+/H447I complex is much more favored than TFK^0/H447I. As shown in Table 2, suppose we have the

TFK^0/H447I complex, the free energy difference of TFK^0 relative to TFK^+ is 20.9 kcal/mol when forming the covalent complex with the H447I mutant (reaction stage) which is overwhelmingly larger than the difference of 7.8 kcal/mol during the diffusion stage. Therefore, thermodynamically speaking, the binding of TFK^0 to the H447I mutant is much less favored, too. In addition, comparing the free energies during the diffusion and reaction stages between the wild-type and H447I mutant (see Table 1), the substantially larger difference during the reaction stage further confirms our QM/MM results.

4. Conclusions

The present calculations suggest a new reaction mechanism for two inhibitors TFK^+ and TFK^0 binding to the H447I mutant mAChE and provide a compelling explanation for the observed different binding behaviors for TFK^+ and TFK^0 in both the wild-type and the H447I mutant mAChEs.

First, our QM/MM calculations of TFK^+ and TFK^0 in wild-type mAChE demonstrate that the bindings of TFK^+ and TFK^0 are spontaneous. The binding of TFK^+ to mAChE contributes an ~27 kcal/mol stabilization to the resulting complex structure, while the binding of TFK^0 causes a nearly 20 kcal/mol energy decrease. These results are consistent with experimental binding affinities of a related series of TMTFA inhibitors.[39]

Second, multiple MD simulations of the $[M-T^+]$ complex consistently show that a water molecule resides in the position originally occupied by His447 in the wild-type mAChE. This water molecule is found to form three stable hydrogen bonds with Ser203, Glu334, and Ser229, respectively. The QM/MM calculations further demonstrate that this water molecule directly participates in the TFK^+ acylation reaction with the enzyme where it acts as a charge relayer, accepting one hydroxyl proton from Ser203 while simultaneously passing one of its protons to the carboxylate of Glu334. However, in the wild-type mAChE, no water was observed to occupy similar positions; therefore, it is unlikely for the wild-type mAChE to adopt such a "charge-relay" reaction mechanism.

Third, multiple MD simulations started from different $[M\cdot T^0]$ models all demonstrate that a stable Ser203, Ser229, and Glu334 triad with a water molecule inside cannot be obtained. No other residue near Ser203 can act as a catalytic base to abstract a hydroxyl proton from Ser203 during the acylation reaction, which explains why TFK^0 is inactive in the H447I mutant.

Finally, we investigated and compared the binding affinities of TFK^+ and TFK^0 in the mAChE using TI calculations. Our result confirms that the complexes $[M\cdot T^+]$ and $[M-T^+]$ are much more stable thermodynamically than the corresponding TFK^0 complexes. And these findings corroborate the above QM/MM calculations and experimental observations.

In conclusion, we explored the TFK^+ and TFK^0 inhibition mechanisms in both the wild-type and H447I mutant mAChEs. Despite the replacement of the catalytic base His447, TFK^+ still demonstrates high binding affinity to the H447I mutant. Our computational studies suggest that a water molecule might act as a "charge relayer" and facilitate the binding of the ligand to the enzyme while this is not true for the binding of the neutral analogue TFK^0. We hope that these results will stimulate further experimental studies.

Acknowledgment. Y.H.C. thanks Prof. Palmer Taylor for helpful discussions and experimental data, and Prof. Yingkai Zhang for advice and access of his QM/MM code and his brilliant idea in simulating enzymatic reactions. This work has been supported in part by grants from the NSF and NIH. Additional support has been provided by NBCR, CTBP, HHMI, the W. M. Keck Foundation, and Accelrys, Inc.

Supporting Information Available: Complete reference information for refs 42 and 56 (S1); Thermodynamic integration calculation details (S2). This material is available free of charge via the Internet at http://pubs.acs.org.

JA070601R